GEOLOGY | THE GEOLOGICAL SOCIETY OF AMERICA®

https://doi.org/10.1130/G51865.1

Manuscript received 6 November 2023
Revised manuscript received 28 January 2024
Manuscript accepted 13 February 2024

Published online 28 February 2024

Fluid environment controls along-strike variation in slip style: Midcrustal geological signatures from the Red River fault, China

Qingbao Duan[1,2,*], Åke Fagereng[2], Jianye Chen[1], and Thomas Blenkinsop[2]
[1]State Key Laboratory of Earthquake Dynamics, Institute of Geology, China Earthquake Administration, Beijing 100029, China
[2]School of Earth and Environmental Sciences, Cardiff University, Cardiff CF10 3AT, UK

ABSTRACT

The slip style of continental midcrustal shear zones plays a crucial role in determining the seismogenic potential of faults, but it remains poorly understood because geological observations that can be directly tied to seismic behavior are scarce. We describe frictional-viscous shear zones in the Red River fault, China, which consists of two segments with distinct seismic behaviors and fluid availabilities. The northern segment hosts moderate to large earthquakes, and midcrustal fault slip is localized into mylonitized pseudotachylyte-bearing layers where dynamically recrystallized quartz records flow stresses exceeding 100 MPa and accelerated viscous creep. The southern segment is dominantly aseismic but active microseismically. Fault slip is accommodated in several mylonitized cataclasite layers, comprising interconnected biotite and intervening fractured clasts, with evidence for pervasive dissolution-precipitation creep. Microstructures, paleopiezometry, and microphysical modeling suggest transient aseismic slip in response to increased strain rates during viscous creep at <50 MPa. We interpret that along-strike variations in fluid environment control fault slip styles and seismic behaviors. The dry and strong northern segment is capable of nucleating large earthquakes, while greater fluid availability in the southern segment activates dissolution-precipitation creep at low driving stresses, which limits interseismic elastic strain accumulation at frictional-viscous transition depths. In this model, compaction-driven fluid pressurization and dilatant hardening are invoked to explain the aseismic slip transients in the southern segment.

INTRODUCTION

Some fault segments creep dominantly aseismically, while others lock between episodic earthquake slip events (Avouac, 2015). In addition, intermediate-speed slip events (slow earthquakes) have been reported from seismic-aseismic transition zones in different tectonic settings (Behr and Bürgmann, 2021; Kirkpatrick et al., 2021). Fundamentally, competition between different mineral-scale deformation mechanisms may control the locked to creeping transition (e.g., Thomas et al., 2014) as well as transient changes in slip speed (Menegon and Fagereng, 2021). However, many parameters, including composition, temperature, effective stress, and strain rate, will affect the spatial transition in slip style (e.g., Janecke and Evans, 1988; Handy et al., 2007; Imber et al., 2008), raising the question: What key parameter controls whether a fault segment is seismic or aseismic? Traditionally, a critical thermal control has been proposed (e.g., Brace and Kohlstedt, 1980); however, it is also clear that the development of phyllosilicates and fluid involvement can lead to profound weakening, strain localization, and potential cyclic interplay between viscous creep and frictional slip within the seismic-aseismic transition zone (Janecke and Evans, 1988; Jefferies et al., 2006; Hardman et al., 2023). Here, we used the midcrustal rock record from seismic and aseismic segments of the Red River fault (RRF), China, to observe variations in structure and composition and infer critical controls on slip style.

GEOLOGICAL SETTING

The RRF extends ∼1000 km from the Eastern Himalayan syntaxis to the South China Sea (Fig. 1A) and has played an important role in accommodating the southeastward extrusion of Tibet (Tapponnier et al., 1990). At least nine historical large earthquakes (M ≥6) have occurred in the northern segment since A.D. 886 (Fig. 1B). In contrast, no large earthquake has occurred in the southern segment during historical or instrumental times. The distribution of small earthquakes (M <5) reveals a seismic gap around the segment boundary. However, given the lack of recent (large) earthquakes and low slip rates constrained by both global positioning system (GPS) data (0.9−1.6 mm/yr; Li et al., 2020) and paleo-earthquakes (∼1.1 mm/yr; Shi et al., 2018), the present-day activity and seismogenic potential of the RRF are still under debate.

Here, we describe pseudotachylyte- and cataclasite-bearing mylonite shear zones from segments of the RRF with distinct seismic behavior. These shear zones are found within the Ailao Shan shear zone (ASSZ; Fig. 1B), which bounds the RRF and which was deformed and exhumed from midcrustal depths by Oligocene–early Miocene left-lateral shear, followed by right-lateral and normal transtension after the late Pliocene (Tapponnier et al., 1990; Searle et al., 2010; Wintsch and Yeh, 2013). The ASSZ rocks experienced amphibolite-facies metamorphism, either before (Searle et al., 2010) or coeval with (Leloup et al., 2001) the left-lateral shear. Most rocks in the ASSZ exhibit steeply dipping, strike-parallel mylonitic foliation and subhorizontal stretching lineation (Liu et al., 2012). The RRF comprises two parallel fault strands: the Range Front fault (RFF) along the northeast flank of the ASSZ and the Mid-Valley fault (MVF) along the Red River valley (Fig. 1C). The RFF accommodated most of the left-lateral and normal faulting components during the exhumation (Replumaz et al., 2001). The MVF accommodated right-lateral slip, as attested by fault scarps and displaced drainage (Replumaz et al., 2001). Deformation and foliation intensi-

Qingbao Duan https://orcid.org/0000-0002-1203-7092
*qbduan@ies.ac.cn

CITATION: Duan, Q., et al., 2024, Fluid environment controls along-strike variation in slip style: Midcrustal geological signatures from the Red River fault, China: Geology, v. XX, p. , https://doi.org/10.1130/G51865.1

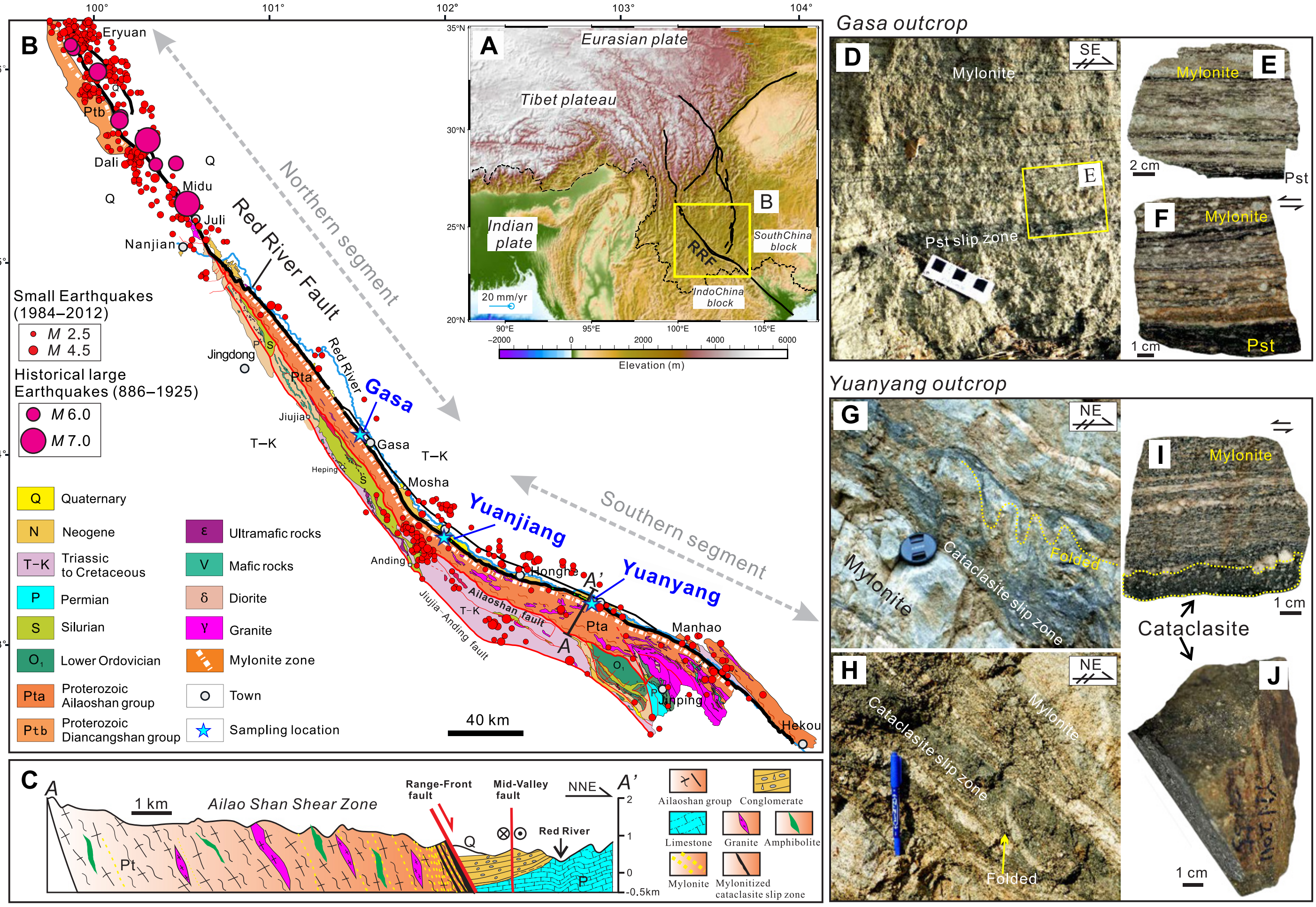

Figure 1. (A) Regional setting of southeast Tibet area. Global positioning system (GPS) data are from Wang and Shen (2020) in Eurasian plate reference frame. (B) Geological map of Red River fault (RRF; after Liu et al., 2012). Small earthquakes are from Li et al. (2020). Historical earthquakes are from Gu et al. (1983). (C) Schematic cross section along profile A–A′. Pt—Proterozoic; Q—Quaternary; P—Permian. (D–F) Photographs of pseudotachylyte (Pst) hosted by mylonites at Gasa. (G–J) Photographs of cataclasites hosted by mylonites at Yuanyang.

ties in the ASSZ show trends of increasing strain toward the RFF. Mylonitized pseudotachylyte and cataclasite slip zones, defined as localized, very high-strain, frictional-viscous deformation zones, developed within mylonites near the RFF (Figs. 1C–1J). We examined these high-strain zones in fault outcrops at Gasa, Yuanjiang, and Yuanyang (Fig. 1B).

MICROSTRUCTURES

At the Gasa outcrop, in the seismic northern segment, centimeter-thick mylonitized pseudotachylyte layers lie parallel to northeast-dipping foliation in granitic mylonites (Figs. 1D–1F; Fig. S1 in the Supplemental Material[1]). These mylonites primarily consist of quartz and feldspars (Figs. 2A and 2B). Vesicles filled with ultrafine-grained biotite crystals are signatures for interpreting the pseudotachylyte (Fig. 2C; Sibson, 1975; Kirkpatrick and Rowe, 2013). Quartz with jagged grain edges that pin into biotite cleavages indicates crystal growth (Fig. 2D). The quartz-quartz boundaries are aligned at high angles to foliated biotite (Fig. 2E), indicating progressive growth and foliation development during subsequent viscous deformation (e.g., Campbell and Menegon, 2019).

At the Yuanjiang outcrop, in the segment boundary, three few-centimeter-thick cataclasite slip zones are parallel to the mylonitic foliation (Fig. S2). The composition and microstructure of these cataclasites are similar to those of the Yuanyang outcrop, in the predominantly aseismic southern segment, where five cataclasite slip zones, several to tens of centimeters thick, are parallel to foliation in mylonites (Figs. 1G–1J; Fig. S3). In these mylonites, dissolution-precipitation creep is recorded by dissolved feldspars and fine-grained neoblasts in stress shadows (Figs. 2F and 2G). Folded quartz veins in mylonitized cataclasites imply cyclical frictional and viscous deformation (Fig. 2H). A local micro–shear zone that formed along interconnected biotite and competent clasts indicates strain incompatibility and stress concentration (Fig. 2I). Solution cleavage defined by biotite wraps around quartz and feldspar clasts (Fig. 2J), and overgrowths in pressure shadows (Fig. 2K) indicate dissolution-precipitation creep. A micrometer-thick slip surface, characterized by vesicles and biotite microlites, and interpreted as a fossilized melt, lies parallel to the foliation in cataclasite matrix (Figs. 2L and 2M; Fig. S4A). The amorphous groundmass and the crystallized biotite have similar compositions to the biotite in cataclasites (Figs. S4B–S4E), suggesting local melting of biotite. Frictional heating is also evidenced by the replacement of biotite by ilmenite along cleavage planes (Fig. 2N). The slip surface is cemented by iron-oxide veins (Figs. S4G–S4I).

DEFORMATION TEMPERATURE, FLOW STRESS, AND STRAIN RATE

Microstructures of quartz ribbons commonly show lobate grain boundaries (Fig. S5), indicat-

[1]Supplemental Material. Method texts, additional figures, and grain-size and mineral chemistry data. Please visit https://doi.org/10.1130/GEOL.S.25219763 to access the supplemental material; contact editing@geosociety.org with any questions.

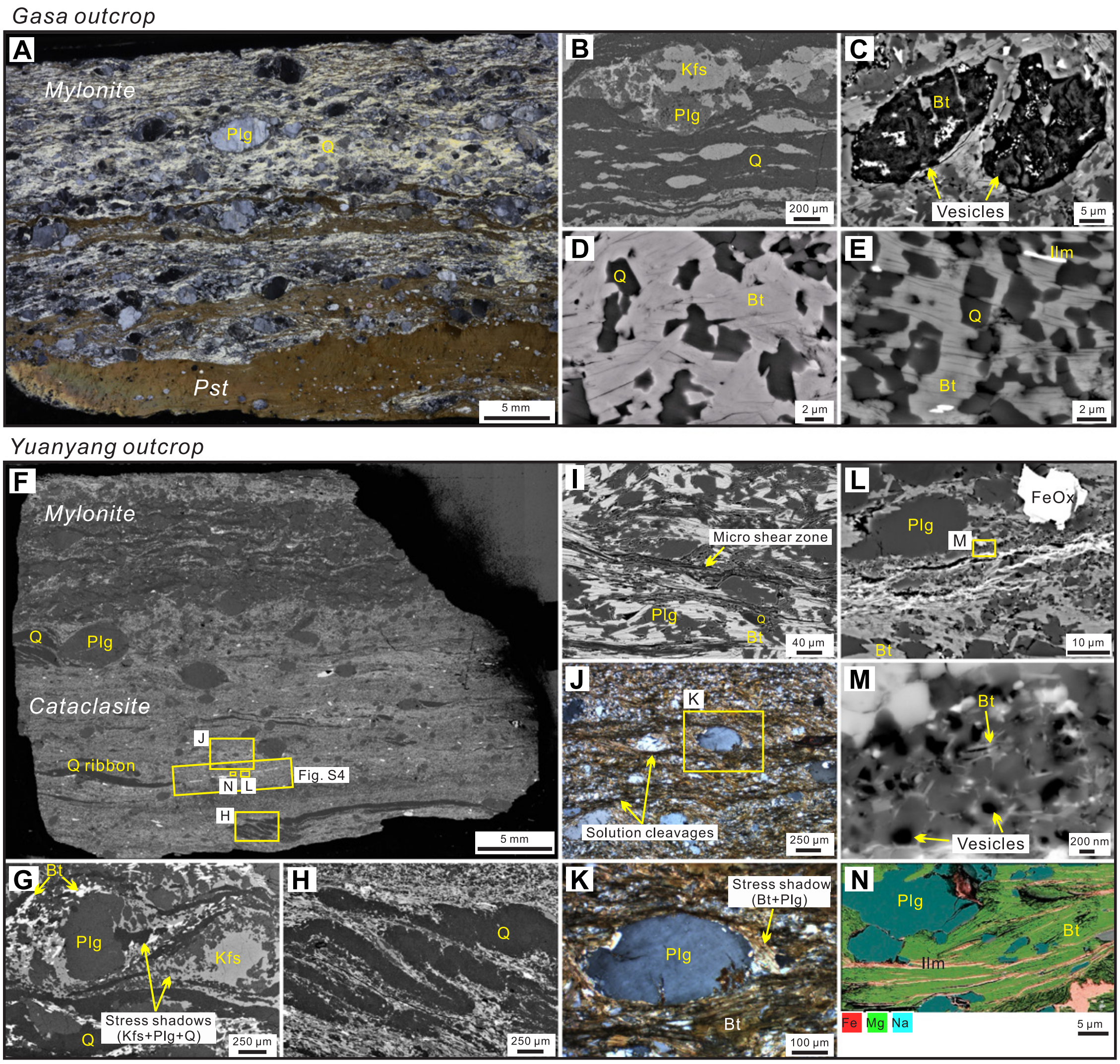

Figure 2. (A) Thin section image of pseudotachylyte (Pst) layer from Gasa (cross-polarized light). (B–E) Backscattered electron (BSE) images of: (B) mylonitic foliation; (C) biotite-filled vesicles; (D) quartz filling voids in biotite cleavage; and (E) biotite foliation with quartz overgrowths. (F) Thin section image of viscously deformed cataclasite from Yuanyang. (G–I) BSE images of: (G) stress shadows adjacent to feldspar clasts; (H) folded quartz vein; (I) micro–shear zone across matrix and clasts. (J–K) Photomicrographs (cross-polarized light) of (J) solution cleavages and (K) close-up of stress shadow with biotite neoblasts. (L) BSE image of localized slip surface in cataclasite, characterized by (M) amorphous texture with vesicles and biotite microlites. (N) Energy-dispersive spectroscopy map of biotite replaced by ilmenite along cleavages. Q—quartz; Plg—plagioclase; Kfs—K-feldspar; Bt—biotite; Ilm—ilmenite; FeOx—iron oxide.

ing the dominance of grain boundary migration recrystallization. Pole figures showing electron backscatter diffraction data (Method Text S1) display point maxima around the kinematic *y* direction (Figs. 3A–3C), with misorientation angles peaking at low angles and misorientation axes clustering around the quartz *c* axis, suggesting prism <*a*> slip (Figs. S6–S8). Maxima between the kinematic *x* and *z* directions (Fig. 3C), along with clustering of misorientation axes around {*m*} and <*a*> (Fig. S6), indicate a prism <*c*> slip system in host rock from Gasa. Although also dependent on strain rate, these data indicate dislocation creep of quartz at relatively high temperatures (>500 °C; Stipp et al., 2002). Application of the Ti-in-biotite geothermometer (Wu and Chen, 2015) to biotite mineral chemistry data (Method Text S2; Table S1; Fig. S9) yielded foliation-forming deformation temperatures of ~650 °C in host rock and ~600 °C near and in slip zones at Gasa (Fig. 3D). At Yuanjiang, the estimated temperatures in the host rock, near the slip zone, and slip zone are ~640 °C, 636 °C, and 622 °C, respectively (Fig. 3E). The estimated temperatures in host rock and slip zone at Yuanyang are slightly colder, at ~610 °C and ~570 °C, respectively (Fig. 3F).

Recrystallized quartz grain sizes decrease toward slip zones and from the southern to northern segment (Figs. 3G–3O). Application of the quartz piezometer of Cross et al. (2017) to grain-size data revealed relatively high flow stresses that increase from 69 MPa in host rock to 145 MPa in slip zones at Gasa (Fig. 4A; Table S2). Flow stresses at Yuanjiang increase from 44 MPa in host rock to 78 MPa in slip zones. At Yuanyang, the flow stresses increase from host-rock flow stress of ~27 MPa to ~49 MPa in slip zones.

Strain rates predicted by a quartz flow law (Lu and Jiang, 2019) at the temperatures from the Ti-in-biotite thermometer fit the paleopiezometry data for 10^{-9}–10^{-8} s^{-1} and 10^{-11}–10^{-10} s^{-1} in the northern and southern segments, respectively (Fig. 4A). Strength curves calculated considering weakening by pressure solution and frictional-viscous slip along biotite cleavages (Bos and Spiers, 2002; Niemeijer and Spiers, 2005; Method Text S4; Table S3) fit well with piezometer-derived flow stresses in the southern segment when bulk strain rates are 10^{-9} s^{-1}–10^{-4} s^{-1} (Fig. 4A). The model predicts a transition in dominant deformation mechanisms from viscous creep to dilatant frictional sliding along biotite cleavages as strain rates increase to ~10^{-4} s^{-1} in cataclasite slip zones.

ALONG-STRIKE VARIATION IN STRESS, STRENGTH, AND SLIP STYLE

The relative scarcity of microstructures that indicate dissolution-precipitation creep and the low phyllosilicate content (Fig. S10A), along with relatively high seismic velocity (Liu et al., 2023) and low electrical conductivity (Ye et al., 2022) at ~20 km depth, indicate that the northern segment was deformed and exhumed in relatively dry conditions. We infer that the relatively dry quartzofeldspathic mylonite is strong enough to host localized high-stress creep and capable of accumulating elastic strain during low-strain-rate interseismic deformation (Figs. 4B–4D). This is supported by the occurrence of large historical earthquakes in the northern segment (Fig. 1B). Whereas the forma-

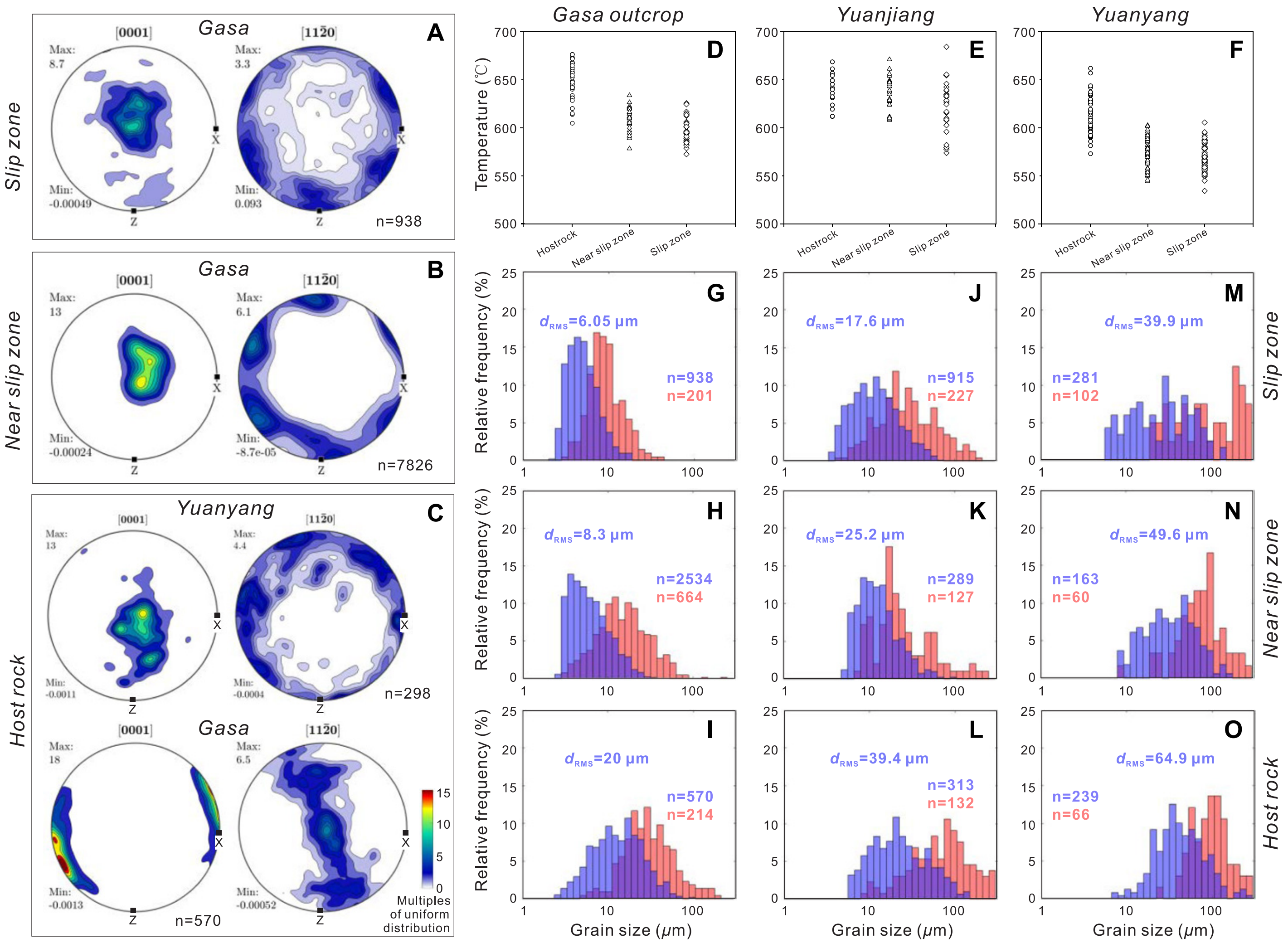

Figure 3. (A–C) Representative pole figures (lower-hemisphere, equal-area projection) of recrystallized quartz. (D–F) Deformation temperature derived by Ti-in-biotite thermometer. (G–O) Grain-size distributions; *n*—number of grains; *dRMS*—root mean square grain size. See Supplemental Material for methods (see text footnote 1).

tion of pseudotachylyte requires seismic slip to have reached the midcrustal rocks, the recorded increase in flow stress from mylonite host rock to mylonitized pseudotachylyte is interpreted to represent transient and localized high-stress, high-strain-rate viscous creep following large earthquakes (Fig. 4B). Similar high-stress transients have been recorded in pseudotachylyte and interpreted as postseismic afterslip in the dry lower crust of Lofoten (Norway) by Campbell and Menegon (2019).

Fault displacement in the southern segment is distributed into a series of viscously deformed cataclasite slip zones. The presence of hydrothermal veins, well-developed pressure solution cleavage, and enrichment in phyllosilicate within the fault-related rocks (Fig. S10B), as well as relatively low seismic velocity (Liu et al., 2023) and high electrical conductivity (Ye et al., 2022) at ~20 km depth, indicate that the southern segment deformed in a fluid-rich environment. These conditions facilitated dissolution-precipitation creep and frictional slip along phyllosilicate foliation (Figs. 2J–2N), enabling deformation at lower stresses (e.g., Janecke and Evans, 1988; Jefferies et al., 2006; Wallis et al., 2015) and higher viscous strain rates, likely suppressing earthquake nucleation by prohibiting elastic strain accumulation during interseismic periods.

In the southern segment, we interpret that the piezometer-derived spatial variations in flow stresses represent transient slips in cataclasite slip zones (Figs. 4B and 4C). Creep-driven fluid pressurization (Menegon and Fagereng, 2021) can explain these slip transients. Fine-grained foliated biotite-rich cataclasite matrix and dissolution cleavages (Fig. 2J) are potential low-permeability seals, causing these slip zones to be poorly drained, thus building up local pressure efficiently during creep compaction. Once the decreasing effective failure strength meets the steady creep driving stress, frictional shear failure will happen (Fig. 4E). Under poorly drained and dilatant conditions, fault slip favors dilatant hardening, where shear-induced dilatation and the associated fluid depressurization prohibit a transition to full instability and limit the slip rate within the aseismic regime (Segall et al., 2010; Chen, 2023). This decrease in fluid pressure also causes a rheological transition back to creep without further frictional failure. The slip transient is cyclical as fluid pressure builds up to trigger new failure episodes with associated fluid depressurization (Fig. 4E), and the rate of fluid pressurization is expected to determine the repeat time. In addition, large earthquakes nucleated in the locked northern segment may impose additional transient loadings on the aseismically slipping southern segment, leading to coherent deformation throughout the fault (Fig. 4D). Therefore, though the southern segment slips dominantly aseismically at frictional-viscous depths, we cannot exclude the possibility that the segment will slip seismically if an external loading increases the strain rate (e.g., Wallis et al., 2015), nor the possibility that this segment imposes elastic loading on the shallower seismogenic zone.

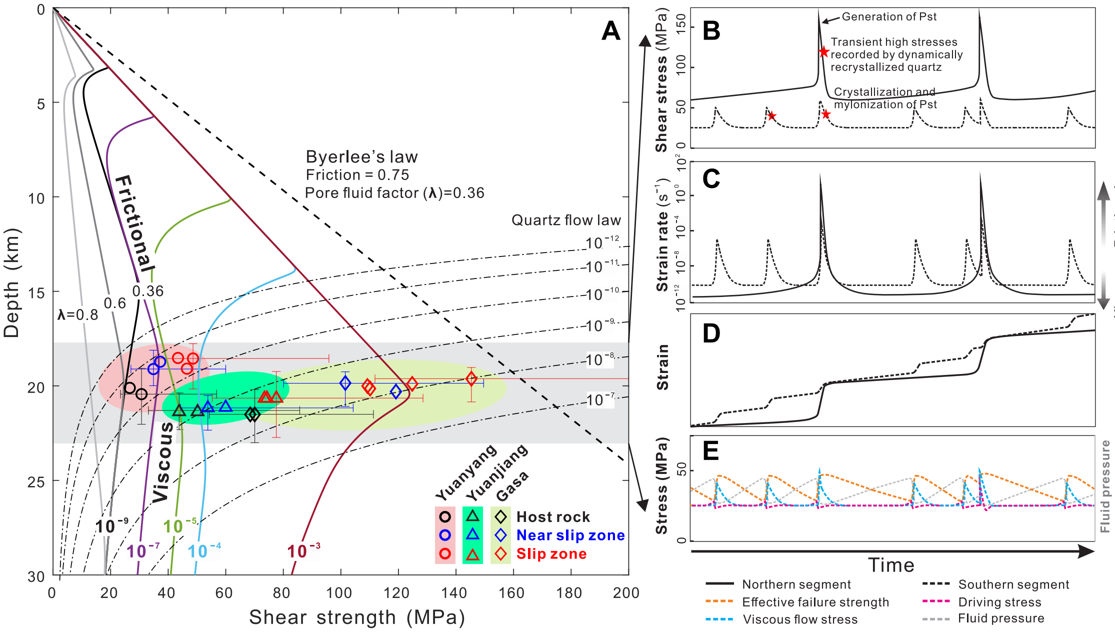

Figure 4. (A) Flow stress estimates and strength curves calculated by microphysical model (Niemeijer and Spiers, 2005; solid curves) and quartz flow law (Lu and Jiang, 2019; dashed curves). Gray shaded area indicates temperature range constrained by Ti-in-biotite thermometer. (B–D) Schematic evolution of (B) stress, (C) strain rate, and (D) strain in northern and southern segments. (E) Schematic evolution of stresses and fluid pressure in southern segment. Pst—pseudotachylyte.

In summary, the northern segment is dominated by episodic large earthquakes at relatively high-stress conditions in a relatively dry crust. The southern segment is dominated by low-stress, aseismic creep, in a fluid-infiltrated crust. The availability of fluids is the overarching control on slip style and may similarly control seismic versus aseismic slip in other faults. We detected local slip surfaces that experienced high, but not seismic, strain rates (~10^{-4} s^{-1}) within the fluid-rich southern segment. We interpret these as examples of creep-driven, transient frictional failure, supporting that this is a mechanism for slow earthquakes within dominantly creeping shear zones.

ACKNOWLEDGMENTS

This study was supported by the National Key Research and Development Program of China (2021YFC3000603) and National Natural Science Foundation of China (42074221). Duan was supported by the China Scholarship Council. Fagereng received funding from the European Research Council Horizon 2020 programme (Starting Grant agreement 715836 "MICA"). The authors acknowledge assistance from Duncan Muir and Xi Ma for scanning electron microscope and electron backscatter diffraction measurements, Tony Oldroyd for thin-section polishing, Jing Xie and Lining Cheng for electron probe microanalysis measurements, and Jinyu Chen and Wenming Yao for fieldwork. We appreciate constructive comments from three anonymous reviewers, which significantly improved the paper.

REFERENCES CITED

Avouac, J.P., 2015, From geodetic imaging of seismic and aseismic fault slip to dynamic modeling of the seismic cycle: Annual Review of Earth and Planetary Sciences, v. 43, p. 233–271, https://doi.org/10.1146/annurev-earth-060614-105302.

Behr, W.M., and Bürgmann, R., 2021, What's down there? The structures, materials and environment of deep-seated slow slip and tremor: Philosophical Transactions of the Royal Society A, v. 379, https://doi.org/10.1098/rsta.2020.0218.

Bos, B., and Spiers, C.J., 2002, Frictional-viscous flow of phyllosilicate-bearing fault rock: Microphysical model and implications for crustal strength profiles: Journal of Geophysical Research, v. 107, p. 1–13, https://doi.org/10.1029/2001JB000301.

Brace, W.F., and Kohlstedt, D.L., 1980, Limits on lithospheric stress imposed by laboratory experiments: Journal of Geophysical Research: Solid Earth, v. 85, p. 6248–6252, https://doi.org/10.1029/JB085iB11p06248.

Campbell, L.R., and Menegon, L., 2019, Transient high strain rate during localized viscous creep in the dry lower continental crust (Lofoten, Norway): Journal of Geophysical Research: Solid Earth, v. 124, p. 10,240–10,260, https://doi.org/10.1029/2019JB018052.

Chen, J.Y., 2023, The emergence of four types of slow slip cycles on dilatant, fluid saturated faults: Journal of Geophysical Research: Solid Earth, v. 128, https://doi.org/10.1029/2022JB024382.

Cross, A.J., Prior, D.J., Stipp, M., and Kidder, S., 2017, The recrystallized grain size piezometer for quartz: An EBSD-based calibration: Geophysical Research Letters, v. 44, p. 6667–6674, https://doi.org/10.1002/2017GL073836.

Gu, G., Lin, T., Shi, Z., Li, Q., Wu, H., Lu, S., Yang, Y., Chen, H., and Wang, S., 1983, The Catalogue of Chinese Earthquakes: Beijing, Science Publishing House [in Chinese].

Handy, M.R., Hirth, G., and Bürgmann, R., 2007, Fault structure and rheology from the frictional-viscous transition downward, *in* Handy, M.R., Hirth, G., and Hovius, N., eds., Tectonic Faults: Agents of Change on a Dynamic Earth: Cambridge, Massachusetts, MIT Press, Dahlem Workshop Report 95, p. 139–181.

Hardman, K., Holdsworth, R.E., Scott, L., Dempsey, E., and McCaffrey, K.J.W., 2023, Mid-crustal reactivation processes linked to frictional melting and deep void development during seismogenic slip: Examples from the Lewisian Complex, NW Scotland: Journal of the Geological Society, v. 180, https://doi.org/10.1144/jgs2022-037.

Imber, J., Holdsworth, R.E., Smith, S.A.F., Jefferies, S.P., and Collettini, C., 2008, Frictional-viscous flow, seismicity and the geology of weak faults: A review and future directions, *in* Wibberley, C.A.J., et al., eds., The Internal Structure of Fault Zones: Implications for Mechanical and Fluid-Flow Properties: Geological Society, London, Special Publication 299, p. 151–173, https://doi.org/10.1144/SP299.10.

Janecke, S.U., and Evans, J.P., 1988, Feldspar-influenced rock rheologies: Geology, v. 16, p. 1064–1067, https://doi.org/10.1130/0091-7613(1988)016<1064:FIRR>2.3.CO;2.

Jefferies, S.P., Holdsworth, R.E., Shimamoto, T., Takagi, H., Lloyd, G.E., and Spiers, C.J., 2006, Origin and mechanical significance of foliated cataclastic rocks in the cores of crustal-scale faults: Examples from the Median Tectonic Line, Japan: Journal of Geophysical Research, v. 111, B12303, https://doi.org/10.1029/2005JB004205.

Kirkpatrick, J.D., and Rowe, C.D., 2013, Disappearing ink: How pseudotachylytes are lost from the rock record: Journal of Structural Geology, v. 52, p. 183–198, https://doi.org/10.1016/j.jsg.2013.03.003.

Kirkpatrick, J.D., Fagereng, Å., and Shelly, D.R., 2021, Geological constraints on the mechanisms of slow earthquakes: Nature Reviews: Earth & Environment, v. 2, p. 285–301, https://doi.org/10.1038/s43017-021-00148-w.

Leloup, P.H., Arnaud, N., Lacassin, R., Kienast, J.R., Harrison, T.M., Trong, T.P., Replumaz, A., and Tapponnier, P., 2001, New constraints on the structure, thermochronology, and timing of the Ailao Shan–Red River shear zone, SE Asia: Journal of Geophysical Research: Solid Earth, v. 106, p. 6683–6732, https://doi.org/10.1029/2000JB900322.

Li, Z., Wang, Y., Gan, W., Fang, L., Zhou, R., Seagren, E.G., Zhang, H., Liang, S., Zhuang, W., and Yang, F., 2020, Diffuse deformation in the SE Tibetan Plateau: New insights from geodetic observations: Journal of Geophysical Research: Solid Earth, v. 125, https://doi.org/10.1029/2020JB019383.

Liu, J., Tang, Y., Tran, M.D., Cao, S., Zhao, L., Zhang, Z., Zhao, Z., and Chen, W., 2012, The nature of the Ailao Shan–Red River (ASRR) shear zone: Constraints from structural, microstructural and fabric analyses of metamorphic rocks from the Diancang Shan, Ailao Shan and Day Nui Con Voi massifs: Journal of Asian Earth Sciences, v. 47, p. 231–251, https://doi.org/10.1016/j.jseaes.2011.10.020.

Liu, Y., Yu, Z., Zhang, Z., Yao, H., Wang, W., Zhang, H., Fang, H., and Fang, L., 2023, The High-Resolution Community Velocity Model V2.0 of southwest China, constructed by joint body and surface wave tomography data recorded at temporary dense arrays: Science China–Earth Sciences, v. 66, p. 2368–2385, https://doi.org/10.1007/s11430-022-1161-7.

Lu, L.X., and Jiang, D., 2019, Quartz flow law revisited: The significance of pressure dependence of the activation enthalpy: Journal of Geophysical Research: Solid Earth, v. 124, p. 241–256, https://doi.org/10.1029/2018JB016226.

Menegon, L., and Fagereng, Å., 2021, Tectonic pressure gradients during viscous creep drive fluid flow and brittle failure at the base of the seismogenic zone: Geology, v. 49, p. 1255–1259, https://doi.org/10.1130/G49012.1.

Niemeijer, A.R., and Spiers, C.J., 2005, Influence of phyllosilicates on fault strength in the brittle-ductile transition: Insights from rock analogue experiments, *in* Bruhn, D., and Burlini, L., eds., High-Strain Zones: Structure and Physical Properties: Geological Society, London, Special Publication 245, p. 303–327, https://doi.org/10.1144/GSL.SP.2005.245.01.15.

Replumaz, A., Lacassin, R., Tapponnier, P., and Leloup, P.H., 2001, Large river offsets and Plio-Quaternary dextral slip rate on the Red River fault (Yunnan, China): Journal of Geophysical Research: Solid Earth, v. 106, p. 819–836, https://doi.org/10.1029/2000JB900135.

Searle, M.P., Yeh, M.W., Lin, T.H., and Chung, S.L., 2010, Structural constraints on the timing of left-lateral shear along the Red River shear zone in the Ailao Shan and Diancang Shan Ranges, Yunnan, SW China: Geosphere, v. 6, p. 316–338, https://doi.org/10.1130/GES00580.1.

Segall, P., Rubin, A.M., Bradley, A.M., and Rice, J.R., 2010, Dilatant strengthening as a mechanism for slow slip events: Journal of Geophysical Research, v. 115, B12305, https://doi.org/10.1029/2010JB007449.

Shi, X., Sieh, K., Weldon, R., Zhu, C., Han, Y., Yang, J., and Robinson, S.W., 2018, Slip rate and rare large prehistoric earthquakes of the Red River fault, southwestern China: Geochemistry, Geophysics, Geosystems, v. 19, p. 2014–2031, https://doi.org/10.1029/2017GC007420.

Sibson, R.H., 1975, Generation of pseudotachylyte by ancient seismic faulting: Geophysical Journal International, v. 43, p. 775–794, https://doi.org/10.1111/j.1365-246X.1975.tb06195.x.

Stipp, M., Stünitz, H., Heilbronner, R., and Schmid, S.M., 2002, Dynamic recrystallization of quartz: Correlation between natural and experimental conditions, *in* De Meer, S., et al., eds., Deformation Mechanisms, Rheology and Tectonics: Current Status and Future Perspectives: Geological Society, London, Special Publication 200, p. 171–190, https://doi.org/10.1144/GSL.SP.2001.200.01.11.

Tapponnier, P., Lacassin, R., Leloup, P.H., Schärer, U., Zhong, D., Wu, H., Liu, X., Ji, S., Zhang, L., and Zhong, J., 1990, The Ailao Shan/Red River metamorphic belt: Tertiary left-lateral shear between Indochina and South China: Nature, v. 343, p. 431–437, https://doi.org/10.1038/343431a0.

Thomas, M.Y., Avouac, J.P., Gratier, J.P., and Lee, J.C., 2014, Lithological control on the deformation mechanism and the mode of fault slip on the Longitudinal Valley fault, Taiwan: Tectonophysics, v. 632, p. 48–63, https://doi.org/10.1016/j.tecto.2014.05.038.

Wallis, D., Lloyd, G.E., Phillips, R.J., Parsons, A.J., and Walshaw, R.D., 2015, Low effective fault strength due to frictional-viscous flow in phyllonites, Karakoram fault zone, NW India: Journal of Structural Geology, v. 77, p. 45–61, https://doi.org/10.1016/j.jsg.2015.05.010.

Wang, M., and Shen, Z.-K., 2020, Present-day crustal deformation of continental China derived from GPS and its tectonic implications: Journal of Geophysical Research: Solid Earth, v. 125, https://doi.org/10.1029/2019JB018774.

Wintsch, R.P., and Yeh, M.W., 2013, Oscillating brittle and viscous behavior through the earthquake cycle in the Red River shear zone: Monitoring flips between reaction and textural softening and hardening: Tectonophysics, v. 587, p. 46–62, https://doi.org/10.1016/j.tecto.2012.09.019.

Wu, C., and Chen, H., 2015, Revised Ti-in-biotite geothermometer for ilmenite- or rutile-bearing crustal metapelites: Science Bulletin, v. 60, p. 116–121, https://doi.org/10.1007/s11434-014-0674-y.

Ye, T., Chen, X., Liu, Z., Wang, P., Dong, Z., Cui, T., Jiang, F., Cai, J., Zhang, Y., Zhang, J., Zhou, L., and Xie, X., 2022, A magnetotelluric study of 3D electrical resistivity structure underneath the southern segment of the Red River fault zone, South China: Journal of Asian Earth Sciences, v. 225, https://doi.org/10.1016/j.jseaes.2021.105056.

Printed in the USA